Electronic field effect detection of SARS-CoV-2 N-protein before the onset of symptoms

I. Novodchuk [a,b,*], M. Kayaharman [b,c], I. Prassas [d], A. Soosaipillai [d], R. Karimi [e], I.A. Goldthorpe [b,c], E. Abdel-Rahman [f], J. Sanderson [e], E.P. Diamandis [d,g], M. Bajcsy [c,h], M. Yavuz [a,b]

[a] Mechanical and Mechatronics Engineering, University of Waterloo, Waterloo, ON, Canada
[b] Waterloo Institute for Nanotechnology (WIN), University of Waterloo, Waterloo, ON, Canada
[c] Department of Electrical and Computer Engineering, University of Waterloo, Waterloo, ON, Canada
[d] Department of Pathology and Laboratory Medicine, Mount Sinai Hospital, Toronto, Canada
[e] Dept. of Physics and Astronomy, University of Waterloo, Waterloo, ON, Canada
[f] Dept. of Systems Design Engineering, University of Waterloo, Waterloo, ON, Canada
[g] Department of Laboratory Medicine and Pathobiology, University of Toronto, Toronto, Canada
[h] Institute for Quantum Computing, University of Waterloo, Waterloo, ON, Canada

ARTICLE INFO

ABSTRACT

As part of the efforts to contain the pandemic, researchers around the world have raced to develop testing platforms to detect the severe acute respiratory syndrome coronavirus 2 (SARS-CoV-2), which causes the Coronavirus disease 2019 (COVID-19). Within the different detection platforms studied, the field effect transistor (FET) is a promising device due to its high sensitivity and fast detection capabilities. In this work, a graphene-based FET which uses a boron and nitrogen co-doped graphene oxide gel (BN-GO gel) transducer functionalized with nucleoprotein antibodies, has been investigated for the detection of SARS-CoV-2 nucleocapsid (N)-protein in buffer. This biosensor was able to detect the viral protein in less than 4 min, with a limit of detection (LOD) as low as 10 ag/mL and a wide linear detection range stretching over 11 orders of magnitude from 10 ag/mL–1 μg/mL. This represents the lowest LOD and widest detection range of any COVID-19 sensor and thus can potentially enable the detection of infected individuals before they become contagious. In addition to its potential use in the COVID-19 pandemic, our device serves as a proof-of-concept of the ability of functionalized BN-GO gel FETs to be used for ultrasensitive yet robust biosensors.

1. Introduction

The severe acute respiratory syndrome coronavirus 2 (SARS-CoV-2) causes the Coronavirus disease 2019 (COVID-19)(Higgins et al., 2020) which was declared a pandemic threat by the World Health Organization in 2020(Seo et al., 2020). One of the significant challenges presented by this virus is that it takes an average of three days for a COVID-19-exposed patient to become contagious, while it takes an average of five days for the symptoms to appear.(Bar-On et al., 2020) SARS-CoV-2 nucleocapsid protein (N-protein) becomes present in saliva post-exposure to COVID-19 and its concentration reaches a peak approximately seven days post-exposure(Shan et al., 2021). Currently, reverse transcriptase polymerase chain reaction (RT-PCR)-based

molecular testing is the main method of testing for COVID-19. Nevertheless, this method has several disadvantages. The nasal swab involved in the sample collection causes significant discomfort to the patient and the test can have a high false-negative rate, especially in the early days of infection(Kucirka et al., 2020). In the real world, and especially during local outbreaks, conventional real-time reverse transcription-polymerase chain reaction (rRT-PCR) testing takes up to 1–3 days between sample collection, shipment to analysis site, laboratory analysis, and reporting(Nguyen et al., 2020). Additionally, the laboratory analysis is expensive and requires highly-trained personnel to operate RT-PCR machine(Parihar et al., 2020).

Other technologies have been developed to combat some of the disadvantages of RT-PCR. The real-time RT-PCR (RT-rtPCR) offers a

limit of detection (LOD) of 200–600 RNA copies/mL and a detection time of up to 3 h(Bezier et al., 2020). Several rapid antigen test devices have emerged and are already in direct-to-consumer routine use in several countries.(Corman et al., 2021) Their applicability for very frequent testing can largely compensate for their relatively reduced sensitivity (compared to traditional molecular PCR-based testing) and they have proven to be indispensable public health tools, especially during local pandemic outbreaks. Commercially available antigen tests can offer a much faster detection time of 15 min but the sensitivity trade-off makes them ineffective for early detection(Green et al., 2020). Therefore, there is a need for a COVID-19 test that would demand minimal sample preparation, have a more sensitive LOD, and give results in a manner of minutes.

Several attempts have been made to reduce the detection time and therefore help control the spread of the disease, using approaches such as immunodiagnostic, digital, and nano-biosensor tests(Mahapatra and Chandra, 2020). While much progress has been made to reduce the detection time to a span of minutes instead of hours or days, LODs remain too high to diagnose patients before they become contagious. Current studies involving nano-biosensors, such as field effect transistors (FETs), are attracting attention due to their fast detection times and good LODs(Seo et al., 2020). Nonetheless, current FETs have either short detection ranges for the SARS-CoV-2 spike protein (1–1000 fg/mL)(Seo et al., 2020) or require sample preparation for RNA testing and do not detect patients before becoming contagious(Li et al., 2021). While extremely sensitive graphene-based FETs have been demonstrated for DNA detection (Mattioli et al., 2021), it has been very difficult to replicate these results for the detection of COVID-19.

In this work, a graphene-based FET was used for the detection of SARS-CoV-2 N-protein in buffer as a proof-of-concept. A boron and nitrogen co-doped graphene oxide (GO) gel (BN-GO gel) transducer functionalized with nucleoprotein antibodies was used, as illustrated in Fig. 1. In graphene-based FETs, there is a critical transition voltage between hole and electron dominant conduction regions, defined as the Dirac point(Mattioli et al., 2021). At the Dirac point, the number of charge carriers in the device is minimal and, therefore, it is compatible for monitoring any changes in the device's environment and attractive for biosensing applications(I. Novodchuk et al., 2021). The Dirac voltage shift in response to N-protein presence was monitored to reveal a highly sensitive response. The device was able to detect N-protein in buffer with a LOD of 10 ag/mL and an incredible detection range of 10 ag/mL-1 µg/mL within minutes, representing both the best LOD and detection range of all COVID-19 biosensors. These results show a great promise towards the detection of COVID-19 patients in all stages of the disease.

2. Experimental

2.1. Materials

Hexagonal boron nitride (h-BN) ultrafine powder and GO solution were purchased from Graphene Supermarket. pH = 7 buffer was purchased from VWR. Ethanolamine was purchased from Sigma Aldrich. SARS-CoV-2 (2019-nCoV) nucleoprotein antibodies (recombinant monoclonal antibody expressed from HEK293 cells of rabbits, Cat #40143-R019) ~50 kDa and SARS-CoV-2 (2019-nCoV) nucleocapsid proteins (His tag) were purchased from Sino Biological. Sino Biological were chosen as the supplier for the n-protein and antibody pair since the pair has already been verified elsewhere (Szabolcs et al., 2021).

2.2. Fabrication of the graphene-based FETs

BN-GO gel FETs were fabricated in the same process as previously reported in Ref (Novodchuk et al., 2020). and (Mistry et al., 2020). In particular, a femtosecond laser ablation was used to fabricate h-BN quantum dots (BNQDs) from an h-BN solution in 50:50 DI water:ethanol. The BNQD solution was mixed with a GO solution and ablated by using pulses from a 1 kHz 35 fs laser with an average power of 1 W. The beam was focused by a 5 cm lens, 2 mm below the surface of the solution for 50 min while constantly stirring using a magnetic stirrer. Post ablation, the solution transformed into a semiconducting gel consisting of B and N co-doped reduced GO (rGO) nanoflakes connected by C–O–C bridges and denoted as BN-GO gel(Novodchuk et al., 2020). The gel was spin-coated between pre-patterned Au/Ti source and drain electrodes on a back-gated SiO_2/p-Si substrate.

2.3. Antibody functionalization and device passivation

2019-nCoV nucleoprotein antibodies were diluted in a pH = 7 buffer
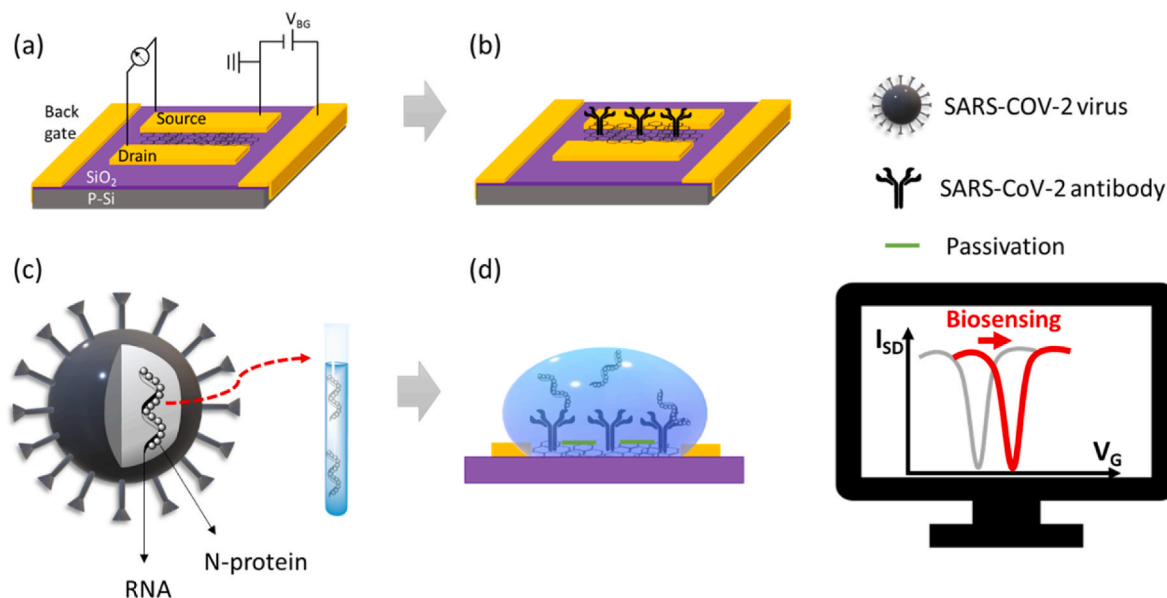
Fig. 1. The schematics of the device configuration and biosensing mechanism of the BN-GO gel FET SARS-CoV-2 N-protein biosensor. (a) The back-gated FET device configuration with the BN-GO gel channel located between the source and drain electrodes. (b) The device configuration after the SARS-CoV-2 antibody functionalization and the passivation with ethanolamine. (c) The N-protein of the SARS-CoV-2 virus is diluted in a buffer solution. (d) The biosensing response is determined based on the shift in the Dirac voltage after the addition of the N-protein-containing solution.

solution to a 10 μg/mL concentration. 5 μL droplets were dropped onto the BN-GO gel channels and left at 4 °C for 48 h, similarly to a previously reported method(I Novodchuk et al., 2021). To passivate the devices in order to prevent unwanted molecules from binding to the BN-GO gel channels during the measurement, the devices were incubated for in 10 mM ethanolamine solution at 4 °C, followed by a thorough rinsing to remove any unbound ethanolamine. The compatibility between the commercial antibodies and N-proteins was confirmed using an enzyme-linked immunosorbent assay (ELISA) test. As comparison, the ELISA test was also conducted for two additional SARS-CoV-2 nucleo-capsid phosphoprotein monoclonal antibodies from a mouse source from two other suppliers (Proteintech and Abcam).

2.4. Immunodetection

All electrical measurements were performed using a probe station setup connected to a software-controlled source measure unit (KEYSIGHT B2900A Series). The SARS-CoV-2 N-protein was serially diluted to multiple concentrations in a 0.1x pH = 7 buffer solution. 2.5 μL of the SARS-CoV-2 N-protein solution with increasing concentrations was dropped onto the antibody-functionalized BN-GO gel channel, and a drain current vs gate voltage plot was obtained after 2 min (at a constant drain voltage of −50 mV). The drain voltage was determined by choosing the maximum charge carrier mobilities for three different drain voltages (−100 mV, −50 mV, and 50 mV) as summarized in Table S1 in the supporting information. −50 mV drain voltage gave the highest charge carrier mobilities. It was found (Novodchuk, 2021) that FET biosensors with higher mobilities can detect analytes at lower LODs. Then the measurement was repeated with a higher concentration of SARS-CoV-2 N-protein solution. The measurement was repeated several times (3–4 times) for each concentration, with a total of 55 measurements taken for two different BN-GO gel FET devices. The results for the buffer solution were taken as the reference. Specificity experiments were performed in the same manner described above, but for unfunctionalized BN-GO gel FET devices. Selectivity experiments were performed in the same manner described, but for different concentrations of K^+ and OH^- solution in a pH = 7 buffer. Additionally, selectivity experiments were repeated for the human epidermal growth factor receptor (HER2) protein, but for a non-passivated sample.

3. Results and discussion

3.1. N-protein concentration in saliva

SARS-CoV-2 N-protein becomes present in saliva post-exposure to COVID-19 and its concentration reaches a peak of ~2000 pg/mL approximately seven days post-exposure(Shan et al., 2021). It is estimated that on the day of the onset of symptoms, (Bar-On, Y.M., Flamholz, A., Phillips, R. and Milo, 2020) the concentration of the viral N-protein in saliva reaches ~70 pg/mL(Shan et al., 2021). However, the patient becomes contagious approximately two days post-exposure, (Bar-On, Y.M., Flamholz, A., Phillips, R. and Milo, 2020) when the concentration of N-protein in saliva is approximately 0.05 pg/mL(Shan et al., 2021). Nevertheless, the most commonly used clinical diagnostic tool, RT-PCR, is unable to detect COVID-19 in the early days and gives a false-negative of 38%–20%(Kucirka et al., 2020).

Table 1 summarizes the patient's contagiousness, N-protein concentration in saliva, and RT-PCR false-negative rate for different days post-exposure to the disease. Based on the data in Table 1, the preferred biosensor would have a limit of detection of the N-protein in saliva much below 50 fg/mL. Also, the detection range should stretch at least over a range of 10 fg/mL- 2 ng/mL. Nonetheless, currently there is no available biosensor that complies with both these parameters(More et al., 2021).

Table 1
N-protein concentration on different days post-exposure, the contagiousness of the patient, and the RT-PCR false-negative rate.

Days since exposure	N-protein concentration in saliva (pg/mL) (Shan et al., 2021)	Is the patient contagious? (Bar-On et al., 2020)	RT-PCR false-negative rate (Kucirka et al., 2020)
7	~2000	Yes	20%
5	~70	Yes	38%
2	~0.05	Yes	100%
1	Unknown	No	100%

3.2. ELISA measurement of SARS-CoV-2 antibody and N-protein

An ELISA test was conducted to confirm the compatibility of the antibody-N-protein pair used in this work (Sino Biological) as compared to other antibody suppliers (Proteintech and Abcam). The ELISA results are presented in Fig. 2. As seen from the figure, only the protein-antibody pair used in this work gives a specific response in the 1–100 ng/mL concentration range. While the specific antibody was from a rabbit source, the non-specific antibodies were from a mouse.

3.3. Antibody functionalization and passivation

BN-GO gel FET devices were fabricated in the same manner as previously described in Ref(I Novodchuk et al., 2021). The channels were incubated in an antibody solution for 48 h at 4 °C. The carboxylic functional groups in the BN-GO gel were demonstrated to covalently capture antibodies through an amine-carboxyl reaction(I Novodchuk et al., 2021). The immobilization of the antibodies was confirmed by the change in the drain current versus gate voltage plot, as demonstrated in Fig. 3. The charge carrier mobilities of these devises reached 360,000 ± 225,000 cm^{2}V^{-1}s^{-1} (n = 7), which are amongst the highest reported for graphene-based materials(Novodchuk, 2021). After immobilization, the Dirac point shifted by approximately −170 mV, and the ON current dropped by at least an order of magnitude. These observations suggest that the antibodies are negatively charged, and the attachment was through covalent bonds which increase charge scattering in the device (Fu et al., 2017). The passivation of the device with ethanolamine caused the Dirac point to shift back towards −50 mV, similar to that of the unfunctionalized BN-GO gel FET.

The antibody immobilization strength was tested by exposing the device to seven consecutive washing cycles, where each cycle consisted of 10 μL of buffer pipetted on and off the channel ten times. After each washing cycle, the drain current of the device was plotted versus the gate voltage (for a drain voltage of – 50 mV), presented in Fig. S1 in the supporting information. As seen from the figure, the Dirac voltage remained constant between the first and the fourth washing cycles, but drastically shifted to −50 mV after the fifth wash cycle, confirming the detachment of antibodies.

3.4. Device configuration and sensing performance

The FET device used in this work consists of a back-gated p-doped silicon wafer with a SiO$_2$ dielectric layer, source and drain electrodes, and a BN-GO gel channel, as illustrated in Fig. 1a. The device is functionalized with SARS-CoV-2 antibodies to specifically detect the SARS-CoV-2 N-proteins in a sample. Then, the device is passivated with ethanolamine to eliminate any undesired charge effects from the sample (Campos et al., 2019), as illustrated in Fig. 1b. In Fig. 1c, the N-proteins of the SARS-CoV-2 virus are diluted in a buffer solution. The drain current versus gate voltage were plotted for a constant back-gate voltage of −50 mV for the antibody-functionalized and passivated BN-GO gel FET in the presence of a buffer solution. This measurement was taken as the reference state where no N-proteins are present in the sample. Then, the diluted sample of N-proteins in buffer was deposited onto the
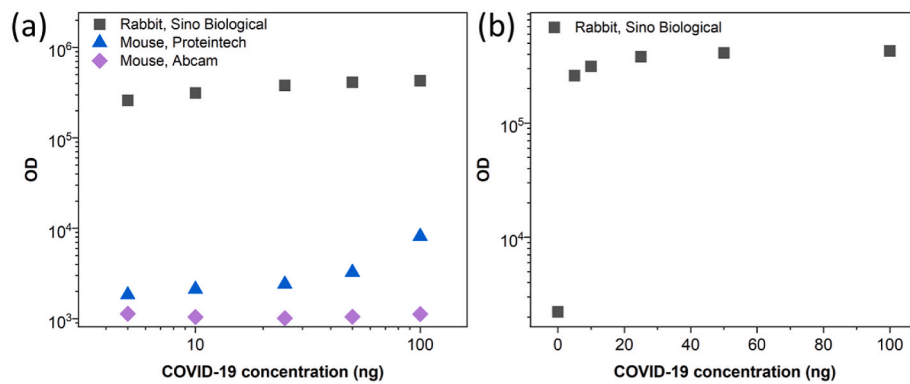
Fig. 2. ELISA results of N-proteins with (a) different commercial antibodies, and (b) the antibodies used in this work. The COVID-19 concentration in (a) is in a logarithmic and (b) a linear scale.
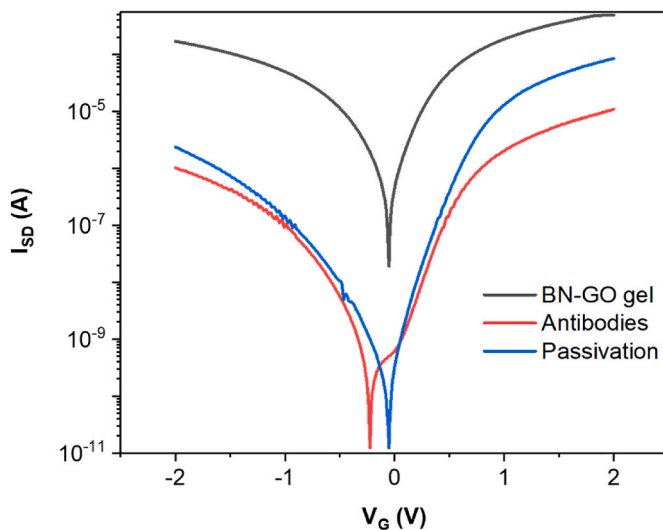
Fig. 3. The change in drain current vs gate voltage plot for a constant drain bias of the BN-GO gel FET after the antibody immobilization and after the passivation with ethanolamine.

channel and the drain current versus gate voltage was recorded. Since the N-proteins have a positive charge (Zeng et al., 2020), their attachment to the antibodies will induce an increase in negative charge in the

BN-GO gel. Thus, the Dirac voltage of the device is expected to increase in response to the N-protein capture, as demonstrated in Fig. 1d.

Fig. 4 presents the BN-GO gel FET biosensor's response to increasing concentrations of SARS-CoV-2 N-proteins (Fig. S2 in the Supporting Information presents the same for lower concentrations). As seen from the figure, while the ON current does not change in response to the N-protein addition, the Dirac point shifts towards higher voltages corresponding to the concentration of the N-protein in the solution. This observation corresponds to that expected for the positively charged N-proteins(Zeng et al., 2020). Additionally, the OFF current decreases with increasing concentrations of the N-proteins. This phenomena stems from the repulsion of positively charged buffer ions from the surface of the channel, reducing any alternative conduction paths(Barua et al., 2021). The LOD of the device was determined as 10 ag/mL, for which the response was larger than 3 times the noise (the average standard deviation for the buffer measurements = 0.02 V).

3.5. Selectivity and specificity

Selectivity and specificity are two important parameters of any biosensor. While the former determines how well the biosensor will recognize the desired molecule while remaining inert to other molecules in the sample (Barua et al., 2021), the latter determines whether the recognition reaction would be solely between the analyte and the bioreceptor(Zhou et al., 2019). To test the specificity of the device, an unfunctionalized and unpassivated BN-GO gel FET was exposed to 10 fg/mL of the N-protein in buffer, as demonstrated in Fig. 5a. This
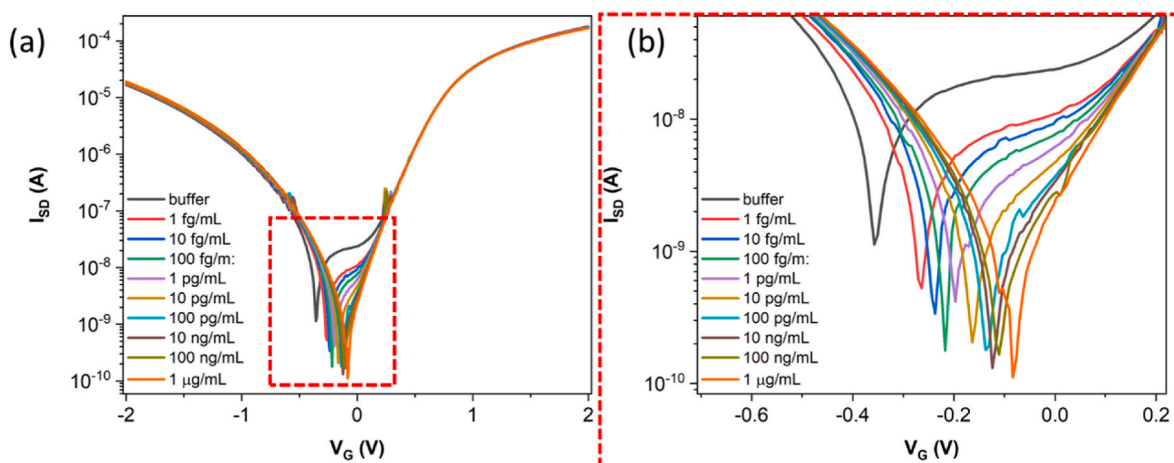
Fig. 4. SARS-CoV-2 N-protein biosensing performance of the antibody-functionalized BN-GO gel FET. (a) The shift in the Dirac voltage in response to increasing concentrations of the N-protein solutions. (b) The magnification of the Dirac points in (a).
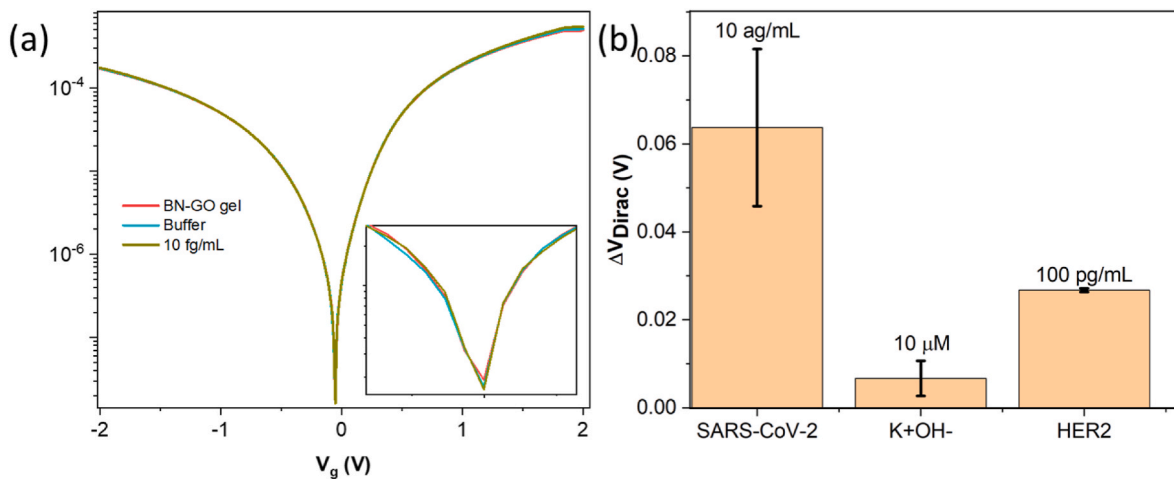
Fig. 5. (a) Specificity and (b) selectivity results for the BN-GO gel FET biosensor. The inset in (a) is a 40x enlargement of the Dirac points.

concentration was chosen since it is three orders of magnitude larger than the LOD of the device. The electrical characteristics of the device have minimal dependence on the presence of the buffer and the 10 fg/mL of the N-protein solution.

The selectivity of the BN-GO gel FET biosensor was tested against K^+ ions and HER2 proteins. These substances were chosen since potassium ions are present in saliva, (Hunter, K. D., & Wilson, 1995) and also since HER2 is a small protein biomarker.(Asgeirsson et al., 2007) The shift in the Dirac voltage in response to different concentrations of potassium ions and HER2 proteins are presented in Fig. S4 a and b in the Supporting Information, respectively.

The selectivity of the device was determined based on the shift in the Dirac voltage in response to different molecules versus the shift for the SARS-CoV-2 N-protein in the LOD concentration (10 ag/mL), as presented in Fig. 5b. As seen in the figure, the shift in the Dirac voltage for the potassium ions solution at a concentration of 10 μM was approximately 7 mV, while the shift in the Dirac voltage for the HER2 solution at a concentration of 100 pg/mL was approximately 27 mV. Both the potassium ions and the HER2 proteins had a much lower effect over the Dirac voltage compared to the N-proteins, with potassium and HER2 giving 9.5- and 2.4-times lower response, respectively. The large difference between the two may stem from the fact that the device was not passivated when tested against the HER2 solution. When comparing the response to the HER2 and the N-proteins solutions at the same concentration (100 pg/mL), the Dirac shift in response to the latter is 7.9 times larger than the former. The authors would like to note that the selectivity studies were done as a proof-of-concept only, Future work aims to target the detection of n-protein in real sample media such as saliva or other bodily fluids.

3.6. Performance compared to the state-of-the-art

As discussed previously, besides the LOD the detection range is another important parameter determining the performance of the biosensor(I. Novodchuk et al., 2021). A biosensor targeting N-protein is required to have a detection range that stretches at least over a range of 50 fg/mL- 2 ng/mL. The shift in the Dirac voltage was extracted for different concentrations of N-proteins in buffer solution and the results are summarized in Fig. 6. As seen from the figure, the detection range stretches over a wide range of concentrations (10 ag/mL – 1 μg/mL), which is at lease 6 orders of magnitude longer than that necessary for the detection of COVID before the patient becomes contagious (Shan et al., 2021). It is also important to note that the relation between the change in the Dirac voltage and the concentration in log scale remained linear and did not reach saturation for the tested concentrations (Seo et al., 2020) indicating that the detection range may be even longer than
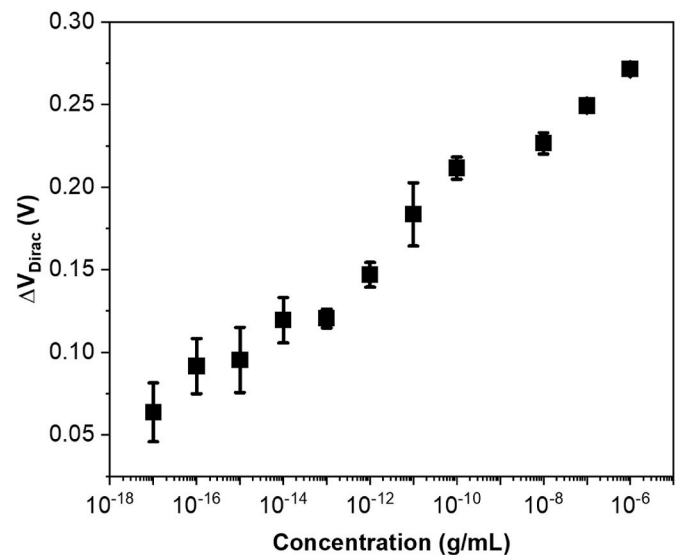
Fig. 6. The shift in the Dirac voltage in response to increasing concentrations of the N-proteins in the solution demonstrates a detection range stretching over 11 orders of magnitude.

originally tested. The results were fitted ($R^2 = 0.98$) with the following relation $\Delta V_{Dirac} = 0.0082*\ln$ (n-protein concentration)+0.3832. This large detection range may be advantageous for the early detection of COVID and for better control over the spread of the disease.

Table 2 compares the biosensing performance of the state-of-the-art FET biosensors targeting the detection of COVID-19. The comparison is based on the biosensing performance for different bioreceptors, transducers, biomarkers, and sample medium. As seen in the table, the current research targets nanomaterials as the transducer material since they demonstrate better signal amplification(Mittal et al., 2017). Specifically, the nanomaterials used as transducers were WSe_2 (Fathi-Hafshejani et al., 2021), and graphene-based materials (reduced graphene oxide decorated with Au nanoparticles (Li et al., 2021) and graphene (Seo et al., 2020)). Interestingly, all the FET biosensors give a very fast detection time, lower than 4 min.

Fathi-Hafshejani et al. (2021) detected the SARS-CoV-2 spike protein in a buffer solution using an antibody-functionalized FET. Their limit of detection was 25 fg/mL, and they reported a wide detection range of six orders of magnitude up to a concentration of 10 ng/mL. The long detection range was a great improvement compared to the first reported FET targeting the detection of COVID-19 which had a detection range of

Table 2
The biosensing performance of the state-of-the-art FET COVID-19 biosensors.

Transducer	Biomarker	Bioreceptor	LOD (pg/mL)	Range (pg/mL)	Medium	Detection time (min)	Ref.
WSe$_2$	SARS-CoV-2 spike protein	Antibody	0.025	0.025–10^4	Buffer	<1 min	Fathi-Hafshejani et al. (2021)
Graphene	SARS-CoV-2 antigen protein	Antibody	0.001 0.1	0.001–1 0.1–10	Buffer Clinical sample	<1 min	Seo et al. (2020)
rGO/Au NPs	RNA	PMO probe	~0.019 (2.29 fM) ~0.032 (3.99 fM)	0.02-10^2 (2 fM-10 pM) 0.03-10^2 (4 fM-10 pM)	Throat swab serum	2 min	Li et al. (2021)
BN-GO gel	**SARS-CoV-2 N-protein**	**Antibody**	**0.00001**	**10^{-5}-10^6**	**Buffer**	**<4 min**	**This work**

1 fg/mL-1 pg/mL of SARS-CoV-2 antigen protein(Seo et al., 2020). In contrast to the previous two papers, Li et al. (2021) targeted the SARS-CoV-2 RNA as their biomarker. They used a reduced rGO transducer decorated with Au nanoparticles (NPs). The complementary phosphorodiamidate morpholino oligos (PMO) probe was immobilized on the Au NPs to selectively capture the biomarkers. The group has demonstrated a low LOD of 0.37 fM in buffer, 2.29 fM in throat swab, and 3.99 fM in serum. Within the biosensors in Table 2, the biosensor discussed in this work is the only one capable of detecting COVID-19 much before the disease becomes contagious, before the onset of symptoms, and at the disease's peak(Shan et al., 2021). Nonetheless, it is important to note that the device has not yet been tested on clinical samples, which commonly reduce the biosensing performance compared to buffer solutions.(Asgeirsson et al., 2007).

4. Summary

In conclusion, we demonstrated the fabrication of a graphene-based FET biosensor capable of the detection of SARS-CoV-2 N-protein in buffer. The transduction relies on a graphene-based semiconductor formed by a BN-GO gel, which was in turn covalently functionalized with SARS-CoV-2 antibodies. Our biosensor device was able to achieve a LOD as little as 10 ag/mL within 4 min. The superior detection range achieved by the biosensor stretched over 11 orders of magnitude (10 ag/mL–1 μg/mL). In addition, the biosensor had minimal response towards interfering species. These results demonstrate high potential towards rapid point-of-care COVID-19 detection using BN-GO gel FET biosensors. The preliminary results demonstrate great promise towards early detection and the potential for effective spread containment. Future experiments should target N-protein detection in more complex matrices, such as saliva or nasal swabs. Additionally, this work serves as a proof-of-principle demonstration of functionalizing the BN-GO gel with antibodies for pathogens and of the potential of BN-GO gel FET to be used in highly sensitive biosensing applications.

Data availability

The raw/processed data required to reproduce these findings cannot be shared at this time due to technical or time limitations.

CRediT authorship contribution statement

I. Novodchuk: Conceptualization, Methodology, Data curation, Writing – original draft. **M. Kayaharman:** Data curation, and Tools. **I. Prassas:** Resources, Data curation, and Analysis – ELISA, Writing – review & editing. **A. Soosaipillai:** Resources, Data curation, and Analysis – ELISA. **R. Karimi:** Resources. **I.A. Goldthorpe:** Resources, Writing – review & editing. **E. Abdel-Rahman:** Resources. **J. Sanderson:** Resources. **E.P. Diamandis:** Resources, Data curation, and Analysis – ELISA. **M. Bajcsy:** Conceptualization, Supervision, Resources, Writing – review & editing. **M. Yavuz:** Conceptualization, Supervision, Resources,

Writing – review & editing.

Declaration of competing interest

The authors declare that they have no known competing financial interests or personal relationships that could have appeared to influence the work reported in this paper.

Appendix A. Supplementary data

Supplementary data to this article can be found online at https://doi.org/10.1016/j.bios.2022.114331.

References

Asgeirsson, K.S., Agrawal, A., Allen, C., Hitch, A., Ellis, I.O., Chapman, C., et al., 2007. Breast Cancer Res. 9 (6), R75.
Bar-On, Y.M., Flamholz, A., Phillips, R., Milo, R., 2020. Elife 9, e57309.
Barua, A., White, R.J., Leedy, K.D., Jha, R., 2021. MRS Commun 11 (3), 233–243.
Bezier, C., Anthoine, G., Charki, A., 2020. Int. J. Metrol. Qual. Eng. 11, 0–16.
Campos, R., Borme, J., Guerreiro, J.R., Machado, G., Cerqueira, M.F., Petrovykh, D.Y., Alpuim, P., 2019. ACS Sens. 4, 286–293.
Corman, V.M., Haage, V.C., Bleicker, T., Schmidt, M.L., Mühlemann, B., Zuchowski, M., Jo, W.K., Tscheak, P., Möncke-Buchner, E., Müller, M.A., Krumbholz, A., 2021. The Lancet Microbe.
Fathi-Hafshejani, P., Azam, N., Wang, L., Kuroda, M.A., Hamilton, M.C., Hasim, S., Mahjouri-Samani, M., 2021. ACS Nano 15 (7), 11461–11469.
Fu, W., Jiang, L., van Geest, E.P., Lima, L.M.C., Schneider, G.F., 2017. Adv. Mater. 29, 1–25.
Green, K., Graziadio, S., Turner, P., Fanshawe, T., Allen, J., 2020. Oxford COVID-19 Evid. Serv 1–12.
Higgins, V., Sohaei, D., Diamandis, E.P., Prassas, I., 2020. Crit. Rev. Clin. Lab Sci. 1–23, 0.
Hunter, K.D., Wilson, W.S., 1995. Arch. Oral Biol. 40, 983–989.
Kucirka, L.M., Lauer, S.A., Laeyendecker, O., Boon, D., Lessler, J., 2020. Ann. Intern. Med. 173, 262–267.
Li, J., Wu, D., Yu, Y., Li, T., Li, K., Xiao, M.M., Li, Y., Zhang, Z.Y., Zhang, G.J., 2021. Biosens. Bioelectron. 183.
Mahapatra, S., Chandra, P., 2020. Biosens. Bioelectron. 165, 112361.
Mattioli, I.A., Hassan, A., Sanches, N.M., Vieira, N.C., Crespilho, F.N., 2021. Biosens. Bioelectron. 175, 112851.
Mistry, K., Ibrahim, K.H., Novodchuk, I., Ngo, H.T., Imamura, G., Sanderson, J., Yavuz, M., Yoshikawa, G., Musselman, K.P., 2020. Adv. Mater. Technol. 2000704
Mittal, S., Kaur, H., Gautam, N., Mantha, A.K., 2017. Biosens. Bioelectron. 88, 217–231.
More, N., Ranglani, D., Kharche, S., Choppadandi, M., Ghosh, S., Vaidya, S., Kapusetti, G., 2021. Meas. Sensors 16, 100052.
Nguyen, T., Bang, D.D., Wolff, A., 2020. Micromachines 11, 1–7.
Novodchuk, I., 2021. Graphene-based FET Biosensors.
Novodchuk, I., Bajcsy, M., Yavuz, M., 2021. Carbon N. Y.
Novodchuk, I., Kayaharman, M., Ausri, I.R., Karimi, R., Tang, X.S., Goldthorpe, I.A., Sanderson, J., Bajcsy, M., Yavuz, M., 2021. Biosens. Bioelectron. 180, 113114.

Novodchuk, I., Kayaharman, M., Ibrahim, K., Al-Tuairqi, S., Irannejad, M., Abdel-Rahman, E., Sanderson, J., Bajcsy, M., Yavuz, M., 2020. Carbon N. Y. 158, 624–630.

Parihar, A., Ranjan, P., Sanghi, S.K., Srivastava, A.K., Khan, R., 2020. ACS Appl. Bio Mater. 3, 7326.

Seo, G., Lee, G., Kim, M.J., Baek, S.H., Choi, M., Ku, K.B., Lee, C.S., Jun, S., Park, D., Kim, H.G., Kim, S.J., Lee, J.O., Kim, B.T., Park, E.C., Kim, S. Il, 2020. ACS Nano 14, 5135–5142.

Shan, D., Johnson, J.M., Fernandes, S.C., Suib, H., Hwang, S., Wuelfing, D., Mendes, M., Holdridge, M., Burke, E.M., Beauregard, K., Zhang, Y., Cleary, M., Xu, S., Yao, X., Patel, P.P., Plavina, T., Wilson, D.H., Chang, L., Kaiser, K.M., Nattermann, J.,

Schmidt, S.V., Latz, E., Hrusovsky, K., Mattoon, D., Ball, A.J., 2021. Nat. Commun. 12.

Szabolcs, M., Sauter, J.L., Frosina, D., Geronimo, J.A., Hernandez, E., Selbs, E., et al., 2021. Appl. Immunohistochem. Mol. Morphol. 29, 5.

Zeng, W., Liu, G., Ma, H., Zhao, D., Yang, Yunru, Liu, M., Mohammed, A., Zhao, C., Yang, Yun, Xie, J., Ding, C., Ma, X., Weng, J., Gao, Y., He, H., Jin, T., 2020. Biophys. Res. Commun. 527, 618–623.

Zhou, L., Wang, K., Sun, H., Zhao, S., Chen, X., Qian, D., Mao, H., Zhao, J., 2019. Nano-Micro Lett. 11 (1), 1–13.